Mathematical Biosciences 224 (2010) 109–117

Contents lists available at ScienceDirect

Mathematical Biosciences

journal homepage: www.elsevier.com/locate/mbs

Activity pattern detection in electroneurographic and electromyogram signals through a heteroscedastic change-point method

M.E. Esquivel-Frausto [a], J.A. Guerrero [b], J.E. Macías-Díaz [c,*]

[a] Departamento de Estadística, Universidad Autónoma de Aguascalientes, Aguascalientes, Ags. 20100, Mexico
[b] Centro de Investigación en Matemáticas, Guanajuato, Gto. 36240, Mexico
[c] Departamento de Matemáticas y Física, Universidad Autónoma de Aguascalientes, Aguascalientes, Ags. 20100, Mexico

ARTICLE INFO

Article history:
Received 29 June 2009
Received in revised form 5 November 2009
Accepted 11 January 2010
Available online 20 January 2010

Keywords:
Change-point estimation
Non-constant variance
Maximum likelihood estimation
Numerical algorithm
Rhythmic pattern activity analysis
Electroneurographic signal

ABSTRACT

In this work, we propose a heteroscedastic method in the detection of activity patterns of electroneurographic and electromyogram signals involved in rhythmic activities of nerves and muscles, respectively. The electric behavior observed in such signals is characterized by phases of activity and silence. The beginning and the length of electrically active and electrically silent phases in a signal allow us to quantitatively analyze the changes and the effects on a rhythmic activity produced by experimental changes. In order to distinguish between these two phases, signals are assumed to be a sample of a time-dependent, normally distributed random variable with non-constant variance, and that the determination of the variance at each point allows us to determine in which phase is the signal. The parameters of the model are determined by means of an iterative process which maximizes the log-likelihood under the proposed model. Moreover, we apply our method to the determination of the activity phases and silence phases in sequences of experimental and synthetic electroneurographic and electromyogram signals. The results obtained with synthetic data show that the method performs well in the determination of these activity patterns. Finally, the study of particular signals simulated under a generalized autoregressive conditional heteroscedasticity model suggests the robustness of the method with respect to the assumption of independence.

1. Introduction

The central generators of rhythmic patterns are parts of the nervous system located mainly in the lower thoracic and lumbar regions of the spinal cord [1]. They are in charge of the coordination of rhythmic movements such as the locomotion, swimming or scratching, and of adjusting them to the physical circumstances. Nerves and muscles taking part in such motions produce an electrical activity which may be measured through electroneurograms or electromyograms, respectively. Such rhythmic activities are characterized by an alternation of periods of electrical activity and electrical inactivity. These two phases are called, respectively, *activity phase* and *silence phase*, and they are typical in electroneurographic (ENG) and electromyogram (EMG) signals, which have been studied extensively in the literature [2–6]

It is important to notice in this point that a rhythmic motion is characterized by the beginning and the duration of the different phases. For instance, Fig. 1 presents a record of the electrical activity of muscles of the hind limbs of a walking cat. The beginning and duration of the phases changes at different rhythms of locomotion, as it is schematically shown in Fig. 2.

It is especially important to calculate the starting moment and the duration of the alternating periods of activity and inactivity in EMG and ENG signals. Thus, the first step in the activity pattern detection is to determine when is the muscle or the nerve of interest in activity, and when is inactive. Several methods have been developed in order to identify activity patterns, including manual methods [7], automatic techniques [8] (included the methods of simple amplitude threshold which find applications in EMG data preprocessed through rectification techniques [9], integration and movable means [10,11], filtered by low-pass filters [12] and wavelets [13]), methods with double threshold [14,15], and change-point techniques [16].

Change-point estimation has been used extensively in the detection of values of sequences where there is a change in the probabilistic distribution of the data. For instance, change-point methods have been proposed for the problem of inferring the time of rejection of transplanted kidneys [17], to analyze the individual

* Corresponding author. Address: Departamento de Matemáticas y Física, Universidad Autónoma de Aguascalientes, Avenida Universidad 940, Colonia Ciudad Universitaria, Aguascalientes, Ags. 20100, Mexico. Tel.: +52 449 910 8400; fax: +52 449 910 8401.
E-mail addresses: mesquive@correo.uaa.mx (M.E. Esquivel-Frausto), antoniog@cimat.mx (J.A. Guerrero), jemacias@correo.uaa.mx (J.E. Macías-Díaz).

0025-5564/$ - see front matter © 2010 Elsevier Inc. All rights reserved.
doi:10.1016/j.mbs.2010.01.001

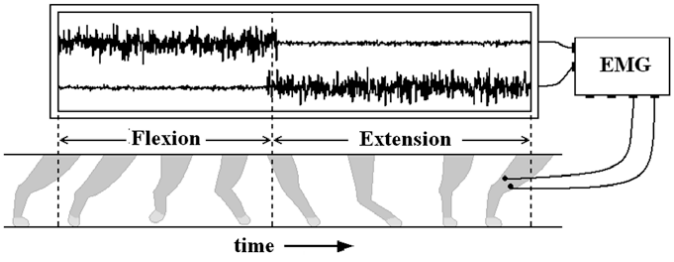

Fig. 1. EMG signals of the flexor and extensor muscles corresponding to the hind limbs of a walking cat.

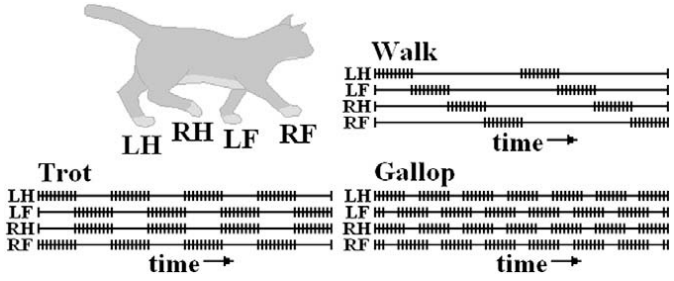

Fig. 2. Patterns of the flexor muscles of the four limbs of a cat at different locomotion speeds: left hind (LH), left front (LF), right hind (RH) and right front (RF).

mechanistic cycle of motor proteins which are crucial to cellular functions [18], to investigate the relationships between benthic diatoms and environmental variables in mid-atlantic highlands [19], to study the electrical discharges of single neurons [20], in the problem of detecting recombinations amongst aligned nucleotide sequences [21] or recombination hot-spots in HIV virus [22], in the investigation of survival data on guinea pigs [23] or problems where the population survival curve is composed of two piecewise exponential functions [24], and even in problems such as the existence of a change-point in a Turkish earthquake data [25] and the change in the annual volume of discharge from the Nile river at Aswan [26]. Here, it is worthwhile mentioning that non-biological areas have also employed successfully change-point techniques in their investigations [27–31].

Nowadays, the specialized literature of the area gives account of many change-point techniques, employing many estimation methods and making use of different statistical or probabilistic assumptions. To provide a brief account of a long story, several change-point methods have successfully employed non-parametric techniques [26,32–34], while others have used maximum likelihood estimation [35–39], and others use a Bayesian approach [40,41,17,30]; conditional techniques have also been used in the change-point analysis of data [42]. Meanwhile, several sets of hypotheses have been employed in the development of new techniques of estimation of a single change-point. For instance, some methods assume that the parametric families involved are known normal [36] or binomial [37] distributions which differ in the numerical values of the parameters or, in general, that the distribution functions are different [43]; other works make use of the assumption that the distributions involved, F and G, satisfy the condition $\int_{\mathbb{R}} G(x)dF(x) \neq \frac{1}{2}$ [44], while others only require for F and G to be different on a set of positive probability [26]. Also, several other methods have been developed in order to detect the presence of multiple change-points [18,45–47].

In this work, we introduce a method of activation pattern detection in ENG and EMG signals. The proposed method includes a segmentation step, in which each point of the signal is assigned to one of two disjoint sets. In this stage, the model parameters are calculated by means of an iterative algorithm which is employed to solve an optimization problem with constraints. The approximate solution obtained in this way is subject to an *a posteriori* treatment in order to eliminate short-length phases which appear due to noise and interference in the recording process of the signals.

Section 2 of this paper presents the mathematical model employed to describe the data of EMG and ENG signals. Basically, we will assume that the observations are samples of normally distributed random variables with mean at the origin and two possible variance values. In Section 3, we introduce the maximum likelihood method used to estimate the times of the signals where there is a change in the activity pattern. In Section 4, an iterative algorithm is presented in order to approximate the optimal value needed in the maximum likelihood method. Next, we present an *a posteriori* procedure in order to avoid short-length phases which are mainly due to noise and interference of the electrical activity in the environment, nearby muscles and readings of the electrical equipment. Section 6 shows the results of applying our detection method to real and synthetic data, including a brief analysis of parametric sensitivity and robustness with respect to the assumption on independence. Meanwhile, the last section of this work gives us a chance to present some conclusions and discussions based on our results.

Before we start our study and for the sake of briefness, we convey that EMG and ENG signals will be simply called 'EMG signals'.

2. Model

An *EMG signal* is a sequence $\boldsymbol{x} = \{x_1, x_2, \ldots, x_n\}$, where each component x_i is a measurement of the electrical activity of a nerve or muscle at a given time t_i. For the sake of simplicity, we may assume that the times in the array $\{t_i\}_{i=1}^n$ are equidistant, that is, that the difference $t_i - t_{i-1}$ is a positive constant independent of the index i. From a statistical point of view, we assume that an EMG signal is actually an independent sample of a sequence of random variables $\{X_i\}_{i=1}^n$, which is an assumption which is reasonably satisfied by our experimental data (see Appendix A). Moreover, we assume that the variables associated to an active phase have a common probability distribution, and the ones associated with a silent phase also have a common (but different) distribution.

In order to determine the parametric distributions that we associate with the activity and the silence phases, it is necessary to point out 'by hand' some of those intervals where each phase is known to occur in the experimental data (see Fig. 3 for data associated to an EMG signal obtained experimentally in the laboratory). This *a priori* analysis is necessary in order to identify the probability distributions of the signals in both phases with some degree of accuracy.

The relative frequency histograms of the points associated to the activity and the silence phases are presented in Fig. 4(a) and (b), respectively. By 'naked eye', it is easy to see that both histograms are unimodal (the mode being a number relatively close to the origin), with mode approximately equal to zero. Moreover, notice that the normal distributions with means and variances

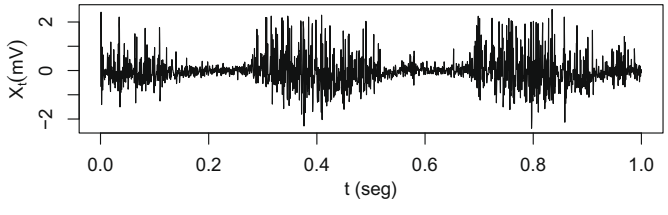

Fig. 3. 2000 samples of a real EMG signal corresponding to a second of rhythmic activity in the locomotion of a cat.

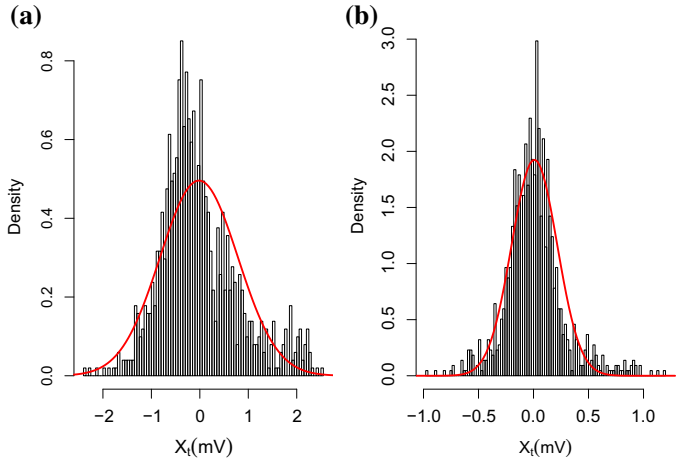

Fig. 4. Histograms of the samples corresponding to an activity phase (left) and a silence phase (right) of the data in Fig. 3. The continuous curve is the graph of a normal distribution with the same mean and variance of the data corresponding to the respective phase.

equal to the corresponding sample means and sample variances of the data, certainly represent a good approximation to the distribution of the points in the case of silence phases, and a reasonable approximation to the distribution of the points in the activity phases. In view of these empirical observations, we propose the normal distribution as the parametric model of the data in each phase. Notationally, we assume that $X_i \sim \mathrm{N}(\mu_i, \sigma_i^2)$, for every $i = 1, 2, \ldots, n$. Moreover, we assume that $\mu_i = 0$ for every i, and that the set of values of the variances σ_i^2 has only two possible choices: σ_a^2 and σ_s^2 (with $\sigma_a^2 > \sigma_s^2$), depending if x_i corresponds to an observation of an activity phase or a silence phase. Summarizing, for every $i = 1, 2, \ldots, n$, we propose the following model for the distribution of the variable X_i:

$$X_i \sim \begin{cases} \mathrm{N}(0, \sigma_s^2), & \text{if there is silence at time } t_i, \\ \mathrm{N}(0, \sigma_a^2), & \text{if there is activity at time } t_i. \end{cases} \tag{1}$$

Let $\boldsymbol{b} = \{b_1, b_2, \ldots, b_n\}$ be a sequence of indicator variables, each b_i being equal to 1 if the muscle is in an activity phase at time t_i, or equal to 0 if it is in a silence phase at that time. Then, (1) may be rewritten as

$$X_i \sim \mathrm{N}(0, b_i\sigma_a^2 + (1 - b_i)\sigma_s^2), \tag{2}$$

for $i = 1, 2, \ldots, n$. In such way, X_i has a normal distribution with mean equal to zero and variance

$$\sigma_i^2 = b_i\sigma_a^2 + (1 - b_i)\sigma_s^2, \tag{3}$$

for every $i = 1, 2, \ldots, n$. In such way, our parametric model is a heteroscedastic process, that is, a random process with non-constant variance.

3. Method

In view that each $b_i \in \{0, 1\}$, it is easy to see that model (2) is equivalent to

$$X_i \sim b_i^2\mathrm{N}(0, \sigma_a^2) + (1 - b_i)^2\mathrm{N}(0, \sigma_s^2), \tag{4}$$

for $i = 1, 2, \ldots, n$. We must mention in advance that both b_i and $1 - b_i$ have been raised to the second power in order to guarantee convergence of the iterative method presented later on in Section 4.

For every $i = 1, 2, \ldots, n$, the log-likelihood of $(b_i, \sigma_a^2, \sigma_s^2)$ is given by

$$\ell(b_i, \sigma_a^2, \sigma_s^2; x_i) = b_i^2\varphi_{\sigma_a^2}(x_i) + (1 - b_i)^2\varphi_{\sigma_s^2}(x_i), \tag{5}$$

where φ_{σ^2} is the logarithm of the density of a normally distributed random variable with mean equal to zero and variance equal to σ^2, that is,

$$\varphi_{\sigma^2}(x) = -\frac{1}{2}\log(2\pi) - \log(\sigma) - \frac{x^2}{2\sigma^2}. \tag{6}$$

Then, the log-likelihood of $(\boldsymbol{b}, \sigma_a^2, \sigma_s^2)$, given the sample $\boldsymbol{x}$, is provided by the identity

$$\ell(\boldsymbol{b}, \sigma_a^2, \sigma_s^2; \boldsymbol{x}) = \sum_{i=1}^{n} \ell(b_i, \sigma_a^2, \sigma_s^2; x_i). \tag{7}$$

Under these circumstances, we denote by $(\boldsymbol{b}_{mle}, \sigma^2_{a,mle}, \sigma^2_{s,mle})$ the maximum likelihood estimators $(\boldsymbol{b}, \sigma_a^2, \sigma_s^2)$, which maximize the function (7).

In view that the components b_i of $\boldsymbol{b}$ are discrete, the determination of $(\boldsymbol{b}_{mle}, \sigma^2_{a,mle}, \sigma^2_{s,mle})$ is a rather difficult task whose solution lies amongst combinatorial techniques. In this article, this difficulty will be avoided by substituting the vectors $\boldsymbol{b}$ for n-dimensional vectors $\tilde{\boldsymbol{b}} = (\tilde{b}_1, \tilde{b}_2, \ldots, \tilde{b}_n)$ consisting of continuous variables. In order for the approximate optimal solution to approach the exact solution $(\boldsymbol{b}_{mle}, \sigma^2_{a,mle}, \sigma^2_{s,mle})$, we will need to impose several conditions on $\tilde{\boldsymbol{b}}$.

First of all, we require that

$$\tilde{b}_i \in [0, 1], \tag{8}$$

for every $i = 1, 2, \ldots, n$. Thus, $\tilde{b}_i$, like its discrete counterpart b_i, indicates whether x_i is an observation corresponding to an activity phase or a silence phase, depending if it takes on a real value approximately equal to 1 or 0, respectively. For this reason, we require that $\tilde{b}_i$ takes on values close to the endpoints of the interval $[0, 1]$, which is equivalent to saying that

$$\tilde{b}_i(1 - \tilde{b}_i) = 0, \tag{9}$$

for every $i = 1, 2, \ldots, n$. Moreover, since the value of the digits b_i remain constant within a phase, and since the only changes occur when there is a transition between phases, we impose the condition that

$$\tilde{b}_i \approx \tilde{b}_{i-1}, \tag{10}$$

for almost all $i = 1, 2, \ldots, n$. It is worth noticing in this point that this last condition does not imply that the variables X_i and X_{i-1} are not independent. In fact, this condition is just a consequence of the fact that X_i and X_{i-1} have the same probability distribution, for almost all $i = 1, 2, \ldots, n$.

In summary, in this work we study the following maximization problem:

$$\begin{aligned} \max_{\tilde{\boldsymbol{b}}, \sigma_a^2, \sigma_s^2} U(\tilde{\boldsymbol{b}}, \sigma_a^2, \sigma_s^2) &= \ell(\tilde{\boldsymbol{b}}, \sigma_a^2, \sigma_s^2; \boldsymbol{x}) \\ &\quad - \omega \sum_{i=1}^{n} \tilde{b}_i(1 - \tilde{b}_i) \\ &\quad - \lambda \sum_{i=2}^{n} (\tilde{b}_i - \tilde{b}_{i-1})^2, \\ \text{s.t.} \quad 0 \leqslant \tilde{b}_i \leqslant 1, &\quad \text{for every} \quad i = 1, 2, \ldots, n. \end{aligned} \tag{11}$$

Constraints (9) and (10) appear as the penalization terms in (11). Meanwhile, the parameters λ and ω are values which are adjusted based on each specific problem.

4. Optimization problem

By differentiating (11) with respect to the model parameters and setting the derivatives equal to zero, we obtain the following expressions for $\tilde{\boldsymbol{b}}$, σ_a^2 and σ_s^2:

$$\tilde{b}_1 = \frac{2\varphi_{\sigma_s^2}(x_1) - 2\lambda\tilde{b}_2 + \omega}{2(\varphi_{\sigma_a^2}(x_1) + \varphi_{\sigma_s^2}(x_1)) - 2\lambda + 2\omega}, \tag{12}$$

$$\tilde{b}_i = \frac{2\varphi_{\sigma_s^2}(x_i) - 2\lambda(\tilde{b}_{i+1} + \tilde{b}_{i-1}) + \omega}{2(\varphi_{\sigma_a^2}(x_i) + \varphi_{\sigma_s^2}(x_i)) - 4\lambda + 2\omega},$$

$$\text{for every } i = 2, \ldots, n-1, \tag{13}$$

$$\tilde{b}_n = \frac{2\varphi_{\sigma_s^2}(x_n) - 2\lambda\tilde{b}_{n-1} + \omega}{2(\varphi_{\sigma_a^2}(x_n) + \varphi_{\sigma_s^2}(x_n)) - 2\lambda + 2\omega}, \tag{14}$$

where

$$\sigma_a^2 = \frac{\sum_{i=1}^n \tilde{b}_i^2 x_i^2}{\sum_{i=1}^n \tilde{b}_i^2}, \tag{15}$$

$$\sigma_s^2 = \frac{\sum_{i=1}^n (1-\tilde{b}_i)^2 x_i^2}{\sum_{i=1}^n (1-\tilde{b}_i)^2}. \tag{16}$$

It is readily seen that Eqs. (15) and (16) depend on $\tilde{\boldsymbol{b}}$, and that (12)–(14) depend on σ_a^2, σ_s^2 and other components of the vector $\tilde{\boldsymbol{b}}$, so that it is hard to obtain an analytical solution to the optimization problem (11). In order to approximate the exact solution, we propose an iterative method in which we assign initial values to $\tilde{\boldsymbol{b}}$, σ_a^2 and σ_s^2, we substitute them into Eqs. (15) and (16), we substitute those new vectors into (12)–(14), and repeat this process until a previously fixed, convergence criterion is satisfied.

In this work, we use the following initial values for σ_a^2 and σ_s^2:

$$\sigma_a^2 = \sigma^2, \tag{17}$$

$$\sigma_s^2 = 0.1\sigma^2, \tag{18}$$

where σ^2 is the variance of all the data in the signal. Moreover, the initial components of the vector $\tilde{\boldsymbol{b}}$ are given by

$$\tilde{b}_i = \frac{\varphi_{\sigma_s^2}(x_i)}{\varphi_{\sigma_a^2}(x_i) + \varphi_{\sigma_s^2}(x_i)}, \tag{19}$$

for every $i = 1, 2, \ldots, n$, which is the optimal solution of the unconstrained version of (11), that is, for $\lambda = \omega = 0$. Moreover, in order to guarantee that condition (8) is satisfied in every step of our method, we use the rule

$$\tilde{b}_i = \begin{cases} 0, & \text{if } \tilde{b}_i < 0, \\ \tilde{b}_i, & \text{if } 0 \leqslant \tilde{b}_i \leqslant 1, \\ 1, & \text{if } \tilde{b}_i > 1. \end{cases} \tag{20}$$

The iterative method to approximate the optimal solution of (11) is summarized in Algorithm 1. The approximate solution with binary components $\hat{\boldsymbol{b}}$ is obtained from $\tilde{\boldsymbol{b}}$ following the rule

$$\hat{b}_i = \begin{cases} 0, & \text{if } \tilde{b}_i \leqslant 0.5, \\ 1, & \text{if } \tilde{b}_i > 0.5, \end{cases} \tag{21}$$

for every $i = 1, 2, \ldots, n$.

5. *A posteriori* processing

The EMG signals exhibit the presence of noise and interference due to electrical activity in the environment, in nearby muscles and in the electrical apparatus employed to measure; moreover, they bring, as a consequence, the presence of short-length phases in $\hat{\boldsymbol{b}}$, as it is shown in the top graph of Fig. 5, which shows the result of applying Algorithm 1 to the data of Fig. 3. In order to get rid of such phases, it is necessary to apply an *a posteriori* processing to $\hat{\boldsymbol{b}}$. Before we explain this process, first we need to introduce a couple of useful operators.

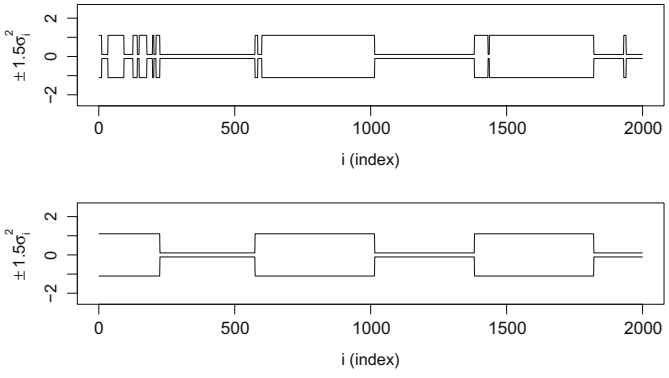

Fig. 5. Graph of $\pm 1.5\sigma_i^2$ as a result of applying Algorithm 1 to the EMG signal of Fig. 3, using the parametric values $\lambda = 100$, $\omega = 1$ and $\epsilon = 0.1$. The results are obtained without employing *a posteriori* processing (top), and employing *a posteriori* processing (bottom), with the parametric values $k_1 = 10$ and $k_2 = 20$.

Given a positive integer k, and a finite sequence of binary numbers $\boldsymbol{y} = (y_1, y_2, \ldots, y_n)$, we define the operators of *dilation* and *erosion* on $\boldsymbol{y}$ by

$$\boldsymbol{\delta}^{(k)}(\boldsymbol{y}) = (\delta^{(k)}(y_1), \delta^{(k)}(y_2), \ldots, \delta^{(k)}(y_n)), \tag{22}$$

$$\boldsymbol{\epsilon}^{(k)}(\boldsymbol{y}) = (\epsilon^{(k)}(y_1), \epsilon^{(k)}(y_2), \ldots, \epsilon^{(k)}(y_n)), \tag{23}$$

respectively, where

$$\delta^{(k)}(y_i) = \max_{j \in N_i^{(k)}} y_j, \tag{24}$$

$$\epsilon^{(k)}(y_i) = \min_{j \in N_i^{(k)}} y_j, \tag{25}$$

for every $i = 1, 2, \ldots, n$, and where $N_i^{(k)}$ is the *set of neighbors* of i with distance k, namely,

$$N_i^{(k)} = \{j : |i-j| \leqslant k\} \cap \{1, 2, \ldots, n\}. \tag{26}$$

Clearly, the dilation and erosion operators have the property that $\boldsymbol{\epsilon}^{(k)}(\boldsymbol{\delta}^{(k)}(\boldsymbol{y}))$ is a finite sequence with no subsequence of zeros of length less than $2k$. In terms of phases, $\boldsymbol{\epsilon}^{(k)}(\boldsymbol{\delta}^{(k)}(\boldsymbol{y}))$ has no silence phase of less than $2k$ samples. Similarly, $\boldsymbol{\delta}^{(k)}(\boldsymbol{\epsilon}^{(k)}(\boldsymbol{y}))$ is a finite sequence which has no subsequence of ones of length less than $2k$, that is, it does not contain an activity phase of length less than $2k$ samples.

Algorithm 1. Detection of activity patterns in EMG signals

input
$\boldsymbol{x} = \{x_1, \ldots, x_n\}$: EMG signal data
ω : parameter of expression associated to (9)
λ : parameter of expression associated to (10)
ϵ : convergence tolerance
begin
Set initial values of σ_a^2 y σ_s^2
Compute $\tilde{b}_i (i = 1, 2, \ldots, n)$ using (19), this estimation is $\tilde{\boldsymbol{b}}^{(0)}$
Let $m = 0$ (iteration number)
repeat
  Increase m by 1
  Update values of σ_a^2 and σ_s^2 using (15) and (16), resp.
  Update $\tilde{\boldsymbol{b}}^{(m-1)}$ using (12)–(14)
  Compute $\tilde{\boldsymbol{b}}^{(m)}$ using (20) on $\tilde{\boldsymbol{b}}^{(m-1)}$
until $\|\tilde{\boldsymbol{b}}^{(m)} - \tilde{\boldsymbol{b}}^{(m-1)}\| < \epsilon$
return $\tilde{\boldsymbol{b}}^{(m)}, \sigma_a^2, \sigma_s^2$

As an estimate of $\boldsymbol{b}$, we propose

$$\epsilon^{(k_1)}(\delta^{(k_1)}(\delta^{(k_2)}(\epsilon^{(k_2)}(\hat{\boldsymbol{b}})))), \tag{27}$$

where the actual values of k_1 and k_2 are parameters which depend on the problem. Fig. 6 shows a schematic representation of the result of the *a posteriori* processing of a binary signal with $k_1 = k_2 = 2$. Fig. 5(b) shows the result of applying the *a posteriori* processing to the signal of Fig. 3. The idea of using Eq. (27) as an estimator of $\boldsymbol{b}$ was actually taken from the theory of image processing (we refer to the description of Fig. 8.55, in p. 486 of [48] for a simple explanation of the effects of the composition of the erosion and dilation operators).

In order to process an EMG signal with a large number of data, Algorithm 1 may be used to find the values of the parameters σ_a^2 and σ_s^2 in a portion of the signal, and then use those values to process the whole signal. This reduces the computation time needed to process the EMG signal, since the computation of σ_a^2 and σ_s^2 is omitted in the iterative algorithm to maximize (11).

6. Experiments

6.1. Simulations

To test the performance of Algorithm 1 with *a posteriori* processing, we possess three EMG signals recorded during the rhythmic activity of scratching of a cat's left ear. The EMG signals correspond to nerves and muscles of the hind limbs of the cat. The top rows of Figs. 7–9 present the graphical representations associated to 1 s. of rhythmic activity (equivalent to 2000 samples, approximately). Meanwhile the bottom rows of those figures show intervals of the form $\pm 1.5\sigma_i^2$, where σ_i^2 is the estimated variance at time t_i, as a result of applying Algorithm 1, using the parameters $\lambda = 100,\ \omega = 1,\ \epsilon = 0.1,\ k_1 = 10$ and $k_2 = 15$.

It is worthwhile noticing that the algorithm seems to be able to detect the activity and the silence phases in the signals. However, it is important to mention also that we do not know if those regions of activity were detected correctly, in view that it is impossible to know the exact starting time and duration of each phase. In order to avoid such shortcoming and measure the performance of the method, we employ the following indicators:

- Percentage of classification error (*PCE*), which is given by

$$PCE = 100 \times \frac{n_E}{n}, \tag{28}$$

where n_E is the number of points where the phase was incorrectly classified (that is, where b_i is incorrectly estimated), and n is the number of samples of the signal.

- Absolute difference in the number of phases (*ADNP*), which is defined by

$$ADNF = |N_f - \widehat{N_f}|, \tag{29}$$

where N_f is the actual number of phases (activity and silence phases) of the signal, and $\widehat{N_f}$ is the number of phases provided by the algorithm.

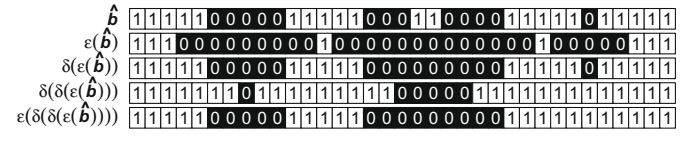

Fig. 6. Example of an application of the *a posteriori* processing of a binary signal (top row) with $k_1 = k_2 = 2$ (the super-indexes have been omitted in order to simplify the expressions). The final result of the *a posteriori* processing is presented at the bottom row of the figure.

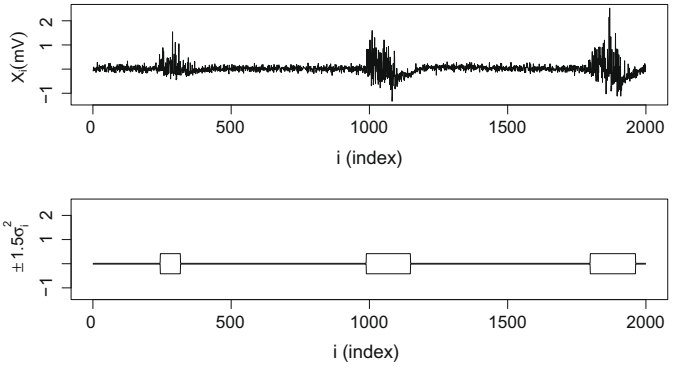

Fig. 7. Data set 1 consisting of experimental EMG signals (top graph) and the corresponding graph of $\pm 1.5\sigma_i^2$ as a result of applying Algorithm 1 with *a posteriori* processing (bottom graph).

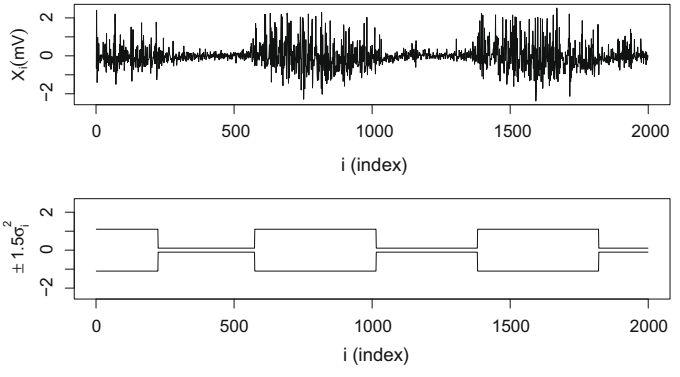

Fig. 8. Data set 2 consisting of experimental EMG signals (top graph) and the corresponding graph of $\pm 1.5\sigma_i^2$ as a result of applying Algorithm 1 with *a posteriori* processing (bottom graph).

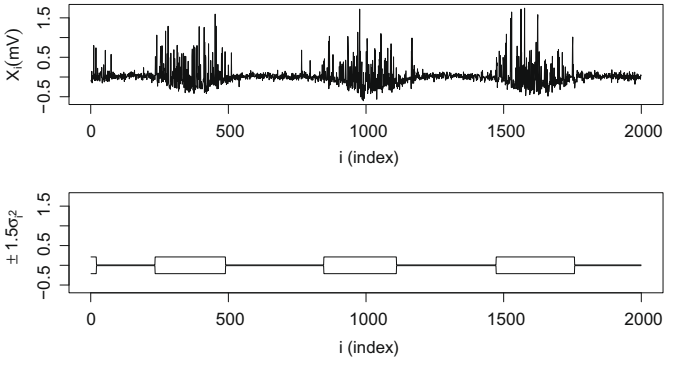

Fig. 9. Data set 3 consisting of experimental EMG signals (top graph) and the corresponding graph of $\pm 1.5\sigma_i^2$ as a result of applying Algorithm 1 with *a posteriori* processing (bottom graph).

In order to test the performance of the algorithm, we employ synthetic data for which the starting point and duration of the activity and the silence phases are known.

For practical purposes, we use signals consisting of 1000 independent samples, such as those presented in Fig. 10. The data were generated randomly with variable periods of activity and silence, all of them approximately equal to 100. The value of σ_a^2 was always equal to 1.0, and σ_s^2 took on the values 0.1, 0.2 and 0.3. For each such value of σ_s^2, 1000 synthetic signals were randomly generated, and the algorithm was applied to each signal using the parameters $\lambda = 100,\ \omega = 1.0,\ \epsilon = 0.1,\ k_1 = 1$ and $k_2 = 15$. Under these circumstances, Fig. 11 presents the graphical results of applying

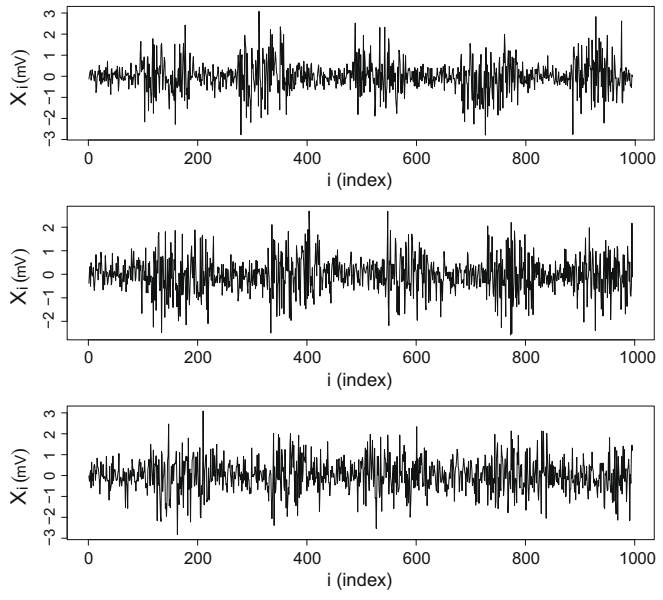

Fig. 10. EMG synthetic data. Each signal consists of 1000 samples during 1 s, with $\sigma_a^2 = 0.1$, and σ_s^2 taking on the values 0.1 (top), 0.2 (middle) and 0.3 (bottom).

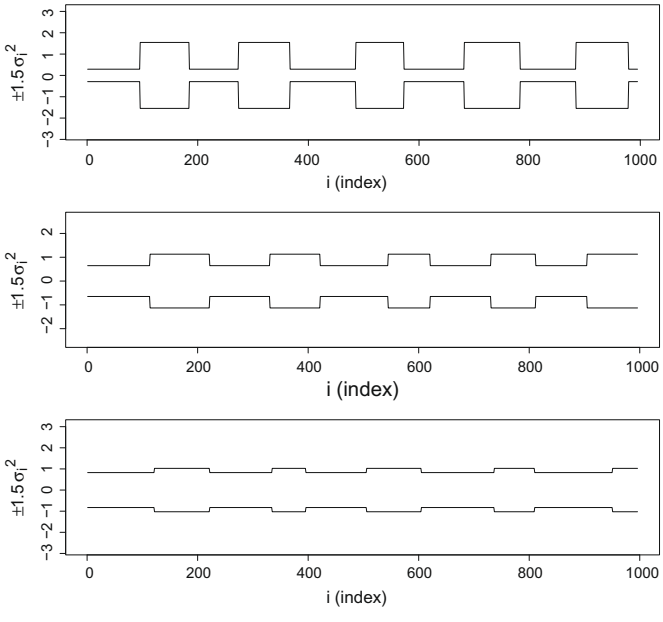

Fig. 11. Graphical results of applying Algorithm 1 with *a posteriori* treatment to each of the synthetic EMS signals presented in Fig. 10. For each of the three signals, the value of $\pm 1.5\sigma_i^2$ has been plotted, where σ_i^2 is the estimated variance of each point.

Algorithm 1 to the signals. By simple inspection one concludes that the method proposed in this work is able to detect the change of phases at a good extent.

To confirm this last claim, Table 1 presents the actual values of *PCE* and *ADNP* associated with each of value of σ_s^2 used. From the results, one can expect that the method will be correct in about 90% of the cases, and that it will be correct in at least 80% of the time. This is by virtue of the fact that the mean *PCE* of the experiments was less than 10%, and that the maximum *PCE* was equal to 19.4. Moreover, in view that the maximum value of *ADNP* is equal to 2, it follows that the algorithm detects correctly the number of activation zones, failing in at most one.

Table 1
Summary of the indicator values *PCE* and *ADNP*, associated with each of the three EMG synthetic signals of Fig. 10, and the corresponding results obtained when applying Algorithm 1 with *a posteriori* processing, presented in Fig. 11.

σ_s^2	*PCE* (%)		*ADNP*	
	Mean	Max	Mean	Max
0.1	3.08	8.2	0.104	2
0.2	6.20	14.0	0.228	2
0.3	9.20	19.4	0.238	2

6.2. Parametric sensitivity

We present now numerical results on the parametric sensitivity of Algorithm 1 with *a posteriori* processing. To that effect, we fix $\sigma_a^2 = 1.0$, and consider three different values of σ_s^2, namely, 0.1, 0.2 and 0.3; moreover, let $k_1 = 1$, $k_2 = 15$ and $\epsilon = 0.1$. Algorithm 1 with *a posteriori* processing is applied then on 3000 synthetic signals, for different values of λ and ω, and the value of the *PCE* is recorded. Here, each phase consists of approximately 100 signals, as before.

Fig. 12 presents the results of our simulations in the form of graphs of level curves, for the three different values of σ_s^2. As we would like to make the *PCE* as small as possible, the graphs of Fig. 12 are useful in order to establish criteria of accuracy in order to correctly classify the phases of activity and silence in an EMG signal. For instance, in the case of $\sigma_s^2 = 0.1$, the optimal *PCE* value is attained at some value of λ within the interval [5,40], and ω in [2.5, 3.0]. Similar qualitative implications may be readily drawn from the graphs corresponding to $\sigma_s^2 = 0.2$ and $\sigma_s^2 = 0.3$.

Before closing this stage of our investigation, it is worth remarking that the results presented in the previous subsection are in perfect agreement with the graphs in Fig. 12. However, the same graphs provide pairs of parametric values for λ and ω that yield optimal *PCE* outcomes, as shown in Table 2. The parameters k_1, k_2 and ϵ are as in the previous paragraphs.

6.3. Robustness

Of course, one of the important assumptions of the method proposed in this work is the independence of the observations. Appendix A establishes that at least there is no strong evidence against the independence of the observations of the signal in Fig. 3. However, an important topic of research is the investigation of the robustness of our method with respect to this rather strong assumption. In view of this, in this section we test our method using a generalized autoregressive conditional heteroscedasticity (GARCH) model [49].

In order to fix notation, the observations ϵ_t under a GARCH model satisfy the property that

$$\epsilon_t = \sigma_t z_t, \tag{30}$$

where the random variables z_t are independent and identically distributed following a standard normal distribution. Moreover, we assume that

$$\sigma_t^2 = \alpha_0 + \sum_{i=1}^{q} \alpha_i \epsilon_{t-i}^2 + \sum_{i=1}^{p} \beta_i \sigma_{t-i}^2. \tag{31}$$

Eq. (31) is the GARCH model of orders p and q, and it is denoted via the nomenclature GARCH(p, q). In our investigation, a GARCH(3, 2) model was fitted to the signal of Fig. 3, and we found that

$$\begin{aligned} \alpha_0 &= 0.009308, \quad \beta_1 = 0.293996, \\ \alpha_1 &= 0.114492, \quad \beta_2 = 0.031293, \\ \alpha_2 &= 0.264180, \quad \beta_3 = 0.290000. \end{aligned} \tag{32}$$

We simulated four signals with the parameters of (32). The results are presented as the four time series of Fig. 13. Next, we applied

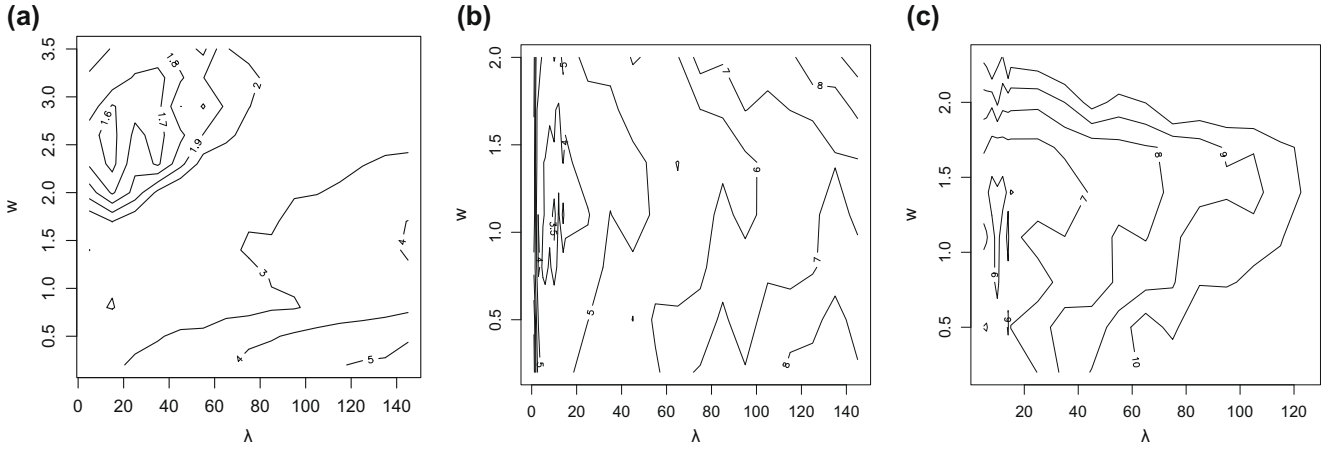

Fig. 12. Graphs of level curves of *PCE* versus λ and ω for 3000 synthetic signals. The results were obtained using Algorithm 1 with *a posteriori* processing, with $\sigma_a^2 = 1.0,\ k_1 = 1,\ k_2 = 15$ and $\epsilon = 0.1$. Three different values of σ_s^2 were employed, namely, (a) 0.1, (b) 0.2 and (c) 0.3. In the synthetic data, each of the phases consisted of approximately 100 signals.

Table 2
Summary of the indicator values *PCE* and *ADNP*, associated with each of three EMG synthetic signals, and the corresponding results obtained when applying Algorithm 1 with *a posteriori* processing.

σ_s^2	Parameters		*PCE* (%)		*ADNP*	
	λ	ω	Mean	Max	Mean	Max
0.1	15	2.5	1.60	5.2	0.316	2
0.2	10	1.0	3.78	10.1	0.387	3
0.3	10	1.5	6.10	19.0	0.749	5

Algorithm 1 with *a posteriori* processing, obtaining the results presented in Fig 13 underneath the graph of each signal.

It is important to notice that the length of each phase depends on the random values z_t, so the occurrence of the change-point is unknown. However, the results obtained through Algorithm 1 seem to indicate that the method performs well detecting activity and silence phases, even in the presence of autoregressive data.

7. Conclusions and discussion

In this article, we have proposed a heteroscedastic model to detect activation patterns in EMG and ENG signals. An iterative procedure to detect the change of patterns was presented, together with an *a posteriori* procedure to avoid short-length phases due to electric noise and interference. In view of the small amount of computational parameters employed by the algorithm (namely, λ, ω, k_1 and k_2), it is easy to adjust these constants in order for the method to be able to estimate the values of the starting point and the length of the activity and the silence phases, as it was evidenced by the sensitivity analysis performed in this work for some particular cases. Our results establish that the algorithm performs well under both synthetic and real signals, and that the method is apparently robust with respect to the independence assumption.

It is interesting to point out that a slight modification of this method is readily at hand, in order to accommodate for the presence of heterogeneous variances $\sigma_{a_1}^2 < \cdots < \sigma_{a_m}^2$ across activity phases, and a common variance $\sigma_{a_0}^2$ in the phases of silence, with $\sigma_{a_0}^2 < \sigma_{a_1}^2$. Indeed, such a general case would be described by the following model for the distribution of probability of X_i:

$$X_i \sim \begin{cases} N(0, \sigma_{a_0}^2), & \text{if there is silence at time } t_i. \\ \mathrm{N}(0, \sigma_{a_k}^2), & \text{if there is activity at time } t_i \\ & \text{with variance equal to } \sigma_{a_k}^2, \\ & \text{for } k = 1, \ldots, m. \end{cases} \tag{33}$$

The model may be conveniently expressed then as

$$X_i \sim \mathrm{N}(0, \sigma_i^2), \tag{34}$$

where the variance σ_i^2 is a suitable linear combination of the variance of the silence phase and the variances of the activity phases. More concretely, σ_i^2 is provided by the formula

$$\sigma_i^2 = \sum_{k=0}^{m} P_k(b_i)\sigma_{a_k}^2, \tag{35}$$

where, for every $k = 0, 1, \ldots, m,\ P_k$ is defined by

$$P_k(x) = \prod_{\substack{j=0 \\ j \neq k}}^{m} \frac{(x-j)}{(k-j)}. \tag{36}$$

In this context, it is easy to check that the advantage of the expression of the function P_k lies in the fact that it is a continuous generalization of the indicator function on k. More precisely, $P_k(x)$ is equal to 1 if and only if $x = k$; moreover, if $x = j$, where $j \in \{0, 1, \ldots, m\} \setminus \{k\}$, then $P_k(x) = 0$. Under these circumstances, a derivation of the technique presented in Section 3 for the case of different variances of the activity phases is feasible. Unfortunately, this modified method assumes the knowledge on the number of such variances, and its validation — which is a topic of further investigation — is outside of the scope of this work. See Guerrero et. al

Finally, it is important to recall that there are several methods in the specialized literature in order to approximate the occurrence of change-points in a time series. For instance, the iterated cumulative sums of squares algorithm introduce in [50] is based on a centered version of the cumulative sum of squares presented in [51], and its properties are justified based on an intuitive basis, as opposed to our algorithm, whose statistical properties are a consequence of employing the method of maximum likelihood estimation. Moreover, the introduction of the *a posteriori* processing is actually a distinctive feature that stands out with respect to many other methods, and not only with respect to the algorithm presented in [50]. As it was shown in this work, *a posteriori* processing is useful in those cases when it is known that the EMG signal under study does not contain phases of activity or silence of relatively short length.

Perhaps one of the most important shortcomings of out technique is the fact that the optimal values of the parameters λ, ω, k_1 and k_2 are not prescribed *a priori*. Even though the analysis of parametric sensitivity establishes the existence of optimal

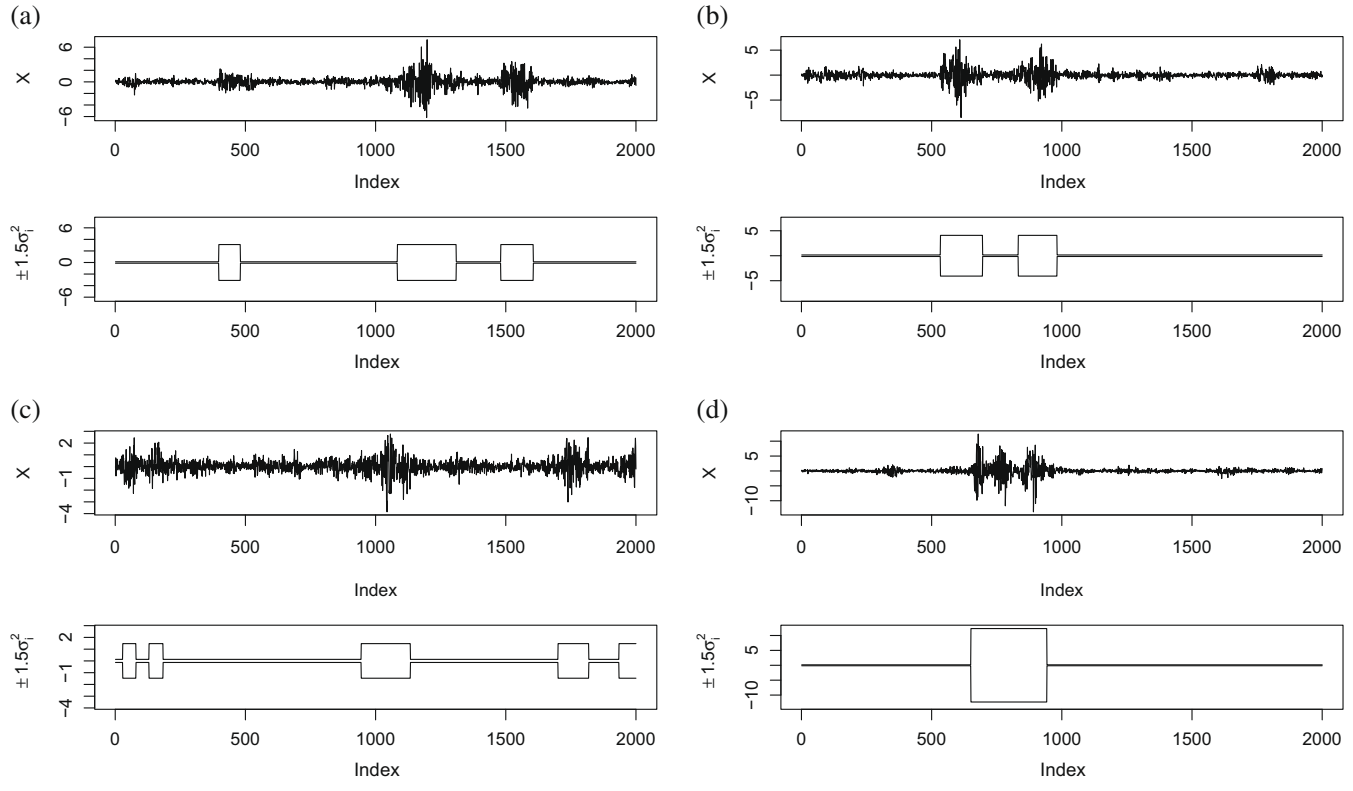

Fig. 13. Four autocorrelated time series obtained under the GARCH model with parameters $p = 3$ and $q = 2$ with coefficients provided by (32), together with the corresponding results of applying Algorithm 1.

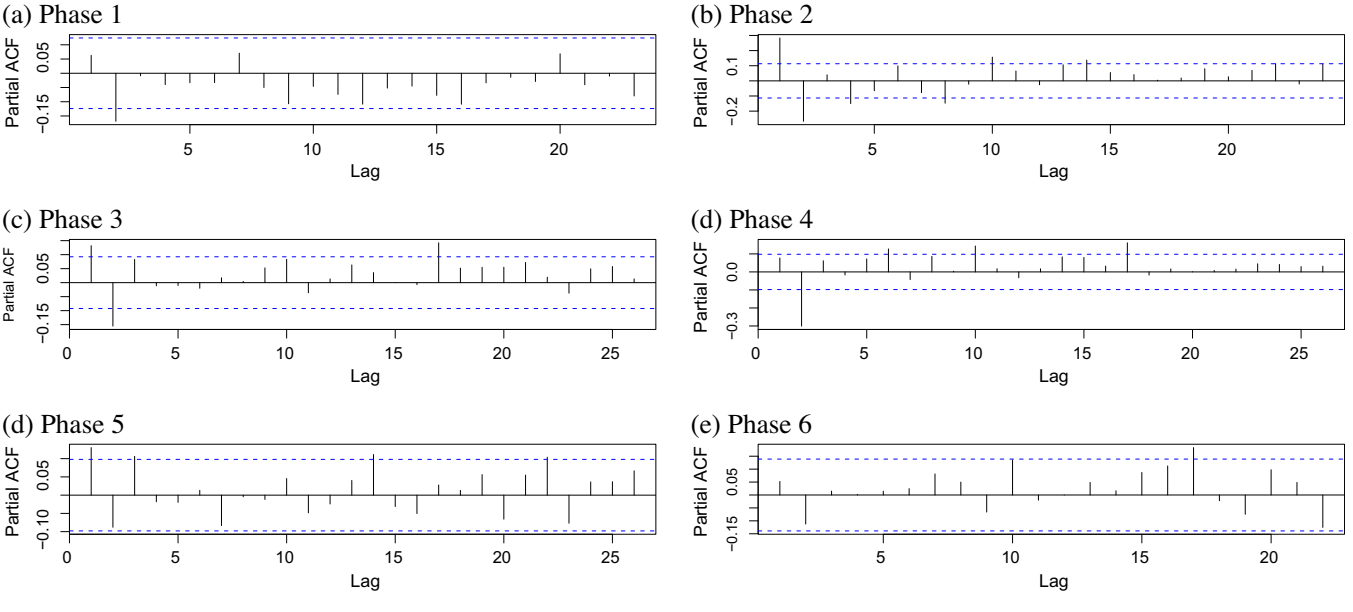

Fig. 14. Graphs of the partial autocorrelation functions of the six phases of the signal shown in Fig. 3. The dotted lines represent the bounds obtained for independent time series with the same parameters as the corresponding signal.

parametric values for λ and ω in the cases considered, it is still unclear if there exists a concrete relationship between such values and the distribution parameters of the signals. Moreover, a deep study on the convergence and the accuracy of the method is still an open topic of further investigation which merits close attention.

Acknowledgments

One of the authors (JEMD) wishes to express his deepest gratitude to Dr. F.J. Álvarez Rodríguez, dean of the Faculty of Science of the Universidad Autónoma de Aguascalientes, and to Dr. F. J. Avelar

González, dean of the Office for Research and Graduate Studies of the same university, for uninterestedly providing the computational resources to produce this article. The authors also wish to thank Dr. L. Castillo-Hernández for providing the experimental data used in this work. Lastly, the authors are indebted to the anonymous reviewers, who provided invaluable comments which led to a great improvement of this work.

Appendix A. Independence in experimental signals

The purpose of this appendix is to show that the experimental data employed to carry out the simulations may be regarded as a time series of approximately independent observations. For instance, let us consider the data of Fig. 3. This time series consists of six phases, three of which are phases of activity and three are phases of silence. The phases of activity occur approximately during the time intervals $I_1 = [0, 0.125]$, $I_3 = [0.2755, 0.5]$ and $I_5 = [0.7005, 0.9]$, while the phases of silence occur in the complementary intervals $I_2 = [0.125, 0.2755]$, $I_4 = [0.5, 0.7005]$ and $I_6 = [0.9, 1]$.

In order to investigate the independence of the data, we have studied the correlation between the observations X_i and X_{i+k} at each I_j, for $j = 1, 2, \ldots, 6$. Fig. 14 presents then the partial autocorrelation functions (see [52] for the definition and properties) of the six phases as a function of the lag term k. Confidence intervals obtained by the simulation of uncorrelated time series are depicted as the regions lying between the horizontal dotted lines in each graph. From the results, we can see that there are very few meaningful correlations (indeed, those which do not lie entirely inside the boundaries obtained for independent samples). Therefore, from a practical point of view, we may state that, even when there is some correlation between the observations, the correlation is not very strong.

References

[1] O. Kiehn, S.J.B. Butt, Physiological, anatomical and genetic identification of CPG neurons in the developing mammalian spinal cord, Prog. Neurobiol. 70 (2003) 347–361.
[2] D. Popivanov, A. Mineva, Testing procedures for non-stationarity and nonlinearity in physiological signals, Math. Biosci. 157 (1999) 303–320.
[3] D. Amarantini, L. Martin, A method to combine numerical optimization and EMG data for the estimation of joint moments under dynamic conditions, J. Biomech. 37 (2004) 1393–1404.
[4] C.C. Gielen, K. van den Oosten, F. Pull ter Gunne, Relation between EMG activation patterns and kinematic properties of aimed arm movements, J. Motor Behav. 17 (1985) 421–442.
[5] J. Navallas, A. Malanda, L. Gila, J. Rodríguez, I. Rodríguez, Mathematical analysis of a muscle architecture model, Math. Biosci. 217 (2009) 64–76.
[6] L. Vigouroux, F. Quaine, A. Labarre-Vila, D. Amarantini, F. Moutet, Using EMG data to constrain optimization procedure improves finger tendon tension estimations during static fingertip force production, J. Biomech. 40 (2007) 2846–2856.
[7] H. Nissen-Petersen, C. Guld, F. Buchthal, A delay line to record random action potentials, Electroencephalogr. Clin. Neurophysiol. 26 (1969) 100–106.
[8] M.B. Raez, M.S. Hussain, F. Mohd-Yasin, Techniques of EMG signal analysis: detection, processing, classification and applications, Biol. Proced. Online 8 (2006) 11–35.
[9] A.J. Thexton, A randomisation method for discriminating between signal and noise in recordings of rhythmic electromyographic activity, J. Neurosci. Meth. 66 (1996) 93–98.
[10] R.A. Bogey, L.A. Barnes, J. Perry, Computer algorithms to characterize individual subject EMG profiles during gait, Arch. Phys. Med. Rehabil. 73 (1992) 835–841.
[11] A.H. Lang, P. Nurkkanen, K.M. Vaahtoranta, Automatic sampling and averaging of electromyographic unit potentials, Electroencephalogr. Clin. Neurophysiol. 31 (1971) 404–406.
[12] J. Perry, E.L. Bontrager, R.A. Bogey, J.K. Gronley, L.A. Barnes, The Rancho EMG analyzer: a computerized system for gait analysis, J. Biomed. Eng. 15 (1993) 487–496.
[13] B. Maimouna, D. Gingras, S. Bédard, D. Langlois, A new method combining wavelet analysis and RBI for gait phases detection in ENG signals, in: 10th Annual Conference of the International FES Society.
[14] P. Bornato, T. d'Alessio, M. Knaflitz, A statistical method for the measurement of muscle activation intervals from surface myoelectric signal during gait, IEEE Trans. Biomed. Eng. 45 (1998) 287–299.
[15] X. Lanyi, A. Adler, An improved method for muscle activation detection during gait, Can. Conf. Electr. Comput. Eng. 1 (2004) 357–360.
[16] T.D. Johnson, R.M. Elashoff, S.J. Harkema, A Bayesian change-point analysis of electromyographic data: detecting muscle activation patterns and associated applications, Biostatistics 4 (2003) 143–164.
[17] A.F.M. Smith, D.G. Cook, Straight lines with a change-point: a Bayesian analysis of some renal transplant data, Appl. Stat. 29 (1980) 180–189.
[18] S.G. Arunajadai, A point process driven multiple change point model: a robust resistant approach, Math. Biosci. 220 (2009) 57–71.
[19] C.L. Weilhoefer, Y. Pan, Using change-point analysis and weighted averaging approaches to explore the relationships between common benthic diatoms and in-stream environmental variables in mid-atlantic highlands, Hydrobiologia 614 (2008) 259–274.
[20] D. Commenges, J. Seal, F. Pinatel, Inference about a change point in experimental neurophysiology, Math. Biosci. 80 (1986) 81–108.
[21] V.N. Minin, K.S. Dorman, F. Fang, M.A. Suchard, Dual multiple change-point model leads to more accurate recombination detection, Bioinformatics 21 (2005) 3034–3042.
[22] V.N. Minin, K.S. Dorman, F. Fang, M.A. Suchard, Phylogenetic mapping of recombination hotspots in human immunodeficiency virus via spatially smoothed change-point processes, Genetics 175 (2007) 1773–1785.
[23] R.C. Gupta, N. Kannan, A. Raychaudhuri, Analysis of lognormal survival data, Math. Biosci. 139 (1997) 103–115.
[24] D. Zelterman, P.M. Grambsch, C.T. Le, J.Z. Ma, Piecewise exponential survival curves with smooth transitions, Math. Biosci. 120 (1994) 233–250.
[25] S. Aktas, H. Konsuk, A. Yîĝîter, Estimation of change point and compound Poisson process parameters for the earthquake data in Turkey, Envirometrics 20 (2008) 416–427.
[26] E. Carlstein, Nonparametric change-point estimation, Ann. Stat. 16 (1988) 188–197.
[27] K.W.K. Andrews, Tests for parameter instability and structural change with unknown change point, Econometrica 61 (1993) 821–856.
[28] S. Chib, Estimation and comparison of multiple change-point models, J. Econ. 86 (1998) 221–241.
[29] C. Pekarik, D.V. Weseloh, Organochlorine contaminants in herring gull eggs from the Great Lakes, 1974–1995: change point regression analysis and short-term regression, Environ. Monitoring Assess. 53 (1998) 77–115.
[30] B. Western, M. Kleykamp, A Bayesian change point model for historical time series analysis, Polit. Anal. 12 (2004) 354–374.
[31] A.F.M. Smith, Change-point problems: approaches and applications, Trabajos Estadíst. Investig. Oper. 31 (1980) 83–89.
[32] A.N. Pettitt, A non-parametric approach to the change-point problem, Appl. Stat. 28 (1979) 126–135.
[33] C.R. Loader, Change point estimation using nonparametric regression, Ann. Stat. 24 (1996) 1667–1678.
[34] E. Carlstein, S. Lele, Nonparametric change-point estimation for data from an ergodic sequence, Theory Probab. Appl. 38 (1993) 726–733.
[35] Y.-X. Fu, R.N. Curnow, Maximum likelihood estimation of multiple change points, Biometrika 77 (1990) 563–573.
[36] D.V. Hinkley, Inference about the change-point in a sequence of random variables, Biometrika 57 (1970) 1–17.
[37] D.V. Hinkley, E.A. Hinkley, Inference about the change-point in a sequence of binomial variables, Biometrika 57 (1970) 477–488.
[38] S. Fotopoulos, V. Jandhyala, Maximum likelihood estimation of a change-point for exponentially distributed random variables, Stat. Probab. Lett. 51 (2001) 423–429.
[39] L. Joseph, D.B. Wolfson, Maximum likelihood estimation in the multi-path change-point problem, Ann. Inst. Stat. Math. 45 (1993) 511–530.
[40] D. Barry, J.A. Hartigan, A Bayesian analysis for change point problems, J. Am. Stat. Assoc. 88 (1993) 309–319.
[41] A.E. Raftery, V.E. Akman, Bayesian analysis of a Poisson process with a change-point, Biometrika 73 (1986) 85–89.
[42] G.W. Cobb, The problem of the Nile: conditional solution to a changepoint problem, Biometrika 65 (1978) 243–251.
[43] D.V. Hinkley, Time-ordered classification, Biometrika 59 (1972) 509–523.
[44] B.S. Darkhovsky, Nonparametric method for the a posteriori detection of the "disorder" time of a sequence of independent random variables, Theory Probab. Appl. 21 (1976) 178–183.
[45] E. Lebarbier, Detecting multiple change-points in the mean of Gaussian process by model selection, Signal Process. 85 (2005) 717–736.
[46] M. Lavielle, G. Teyssière, Detection of multiple change-points in multivariate time series, Lithuanian Math. J. 46 (2006) 287–306.
[47] M. Lavielle, C. Ludeña, The multiple change-points problem for the spectral distribution, Bernoulli 6 (2000) 845–869.
[48] J.C. Russ, The Image Processing Handbook, fifth ed., CRC Press, Boca Raton, FL, 2007.
[49] T. Bollerslev, Generalized autoregressive conditional heteroskedasticity, J. Econ. 31 (1986) 307–327.
[50] C. Inclán, G.C. Tiao, Use of cumulative sums of squares for retrospective detection of changes of variance, J. Am. Stat. Assoc. 89 (1994) 913–923.
[51] R.L. Brown, J. Durbin, J. M Evans, Techniques for testing the constancy of regression relationships over time, J. Roy. Stat. Soc., Ser. B 37 (1975) 149–163.
[52] G.E.P. Box, G.M. Jenkins, G.C. Reinsel, Time Series Analysis, Forecasting and Control, third ed., Prentice Hall, Englewood Clifs, NJ, 1994.